Available online at https://link.springer.com/journal/42241
http://www.jhydrodynamics.com
Journal of Hydrodynamics, 2021, 33(2): 195-206
https://doi.org/10.1007/s42241-021-0031-y

A CAD-compatible body-fitted particle generator for arbitrarily complex geometry and its application to wave-structure interaction *

Yujie Zhu[1], Chi Zhang[1], Yongchuan Yu[2], Xiangyu Hu[1]
1. *Department of Mechanical Engineering, Technical University of Munich, Garching, Germany*
2. *Department of Aerospace and Geodesy, Technical University of Munich, Taufkirchen, Germany*

(Received April 8, 2021, Revised April 12, 2021, Accepted April 13, 2021, Published online April 28, 2021)

Abstract: Generating body-fitted particle distribution for arbitrarily complex geometry underpins the applications of particle-based method to engineering and bioengineering and is highly challenging, and thus hinders the potential of particle methods. In this paper, we present a new computer-aided design (CAD) compatible body-fitted particle generator, termed as CAD-BPG, for arbitrarily complex 3-D geometry. By parsing a CAD model, the present method can accurately tackle arbitrarily complex geometry representation and describe the corresponding geometry surface by constructing an implicit zero level-set function on Cartesian background mesh. To achieve a body-fitted and isotropic particle distribution, physics-driven relaxation process with surface bounding governed by the transport-velocity formulation of smoothed particle hydrodynamics (SPH) methodology is conducted to characterize the particle evolution. A set of examples, ranging from propeller, stent structures and anatomical heart models, show simplicity, accuracy and versatility of the present CAD-BPG for generating body-fitted particle distribution of arbitrarily complex 3-D geometry. Last but not least, the present CAD-BPG is applied for modeling wave-structure interaction, where wave interaction with an oscillating wave surge converter is studied, and the results show that the present method not only provides an efficient and easy-to-implement pre-processing tool for particle-based simulation but also improves the numerical accuracy compared with lattice particle distribution. Consequently, the propose CAD-BPG sheds light on simulating real-world applications by particle-based methods for researchers and engineers.

Key words: CAD-compatible, body-fitted, particle distribution, level-set

Introduction

Fully Lagrangian mesh free particle-based methods, in particular smoothed particle hydrodynamics (SPH)[1-2], moving-particle semi-implicit method (MPS)[3] and discrete element method (DEM)[4], have attracted increasing attention in a broad range of fields including fluid dynamics[5-9], solid mechanics[10-13] and fluid structure interactions[14-16]. In the past decades, particle-based methods have been applied in industrial applications where complex 3-D geometry are involved, viz, bird strike[17], high-pressure water jets impacting pelton turbine blades[18], oil flow inside a gearbox[19], wave-structure interactions[20-21] and stent and myocardium deformation in biomechanics[22-23]. These industrial and biomechanical applications pose a challenge of generating high-quality body-fitted particle distribution for arbitrarily complex 3-D geometry.

In particle-based methods, initial particle distribution is commonly generated by two approaches: (1) direct initiate particles on a lattice structure, (2) generate particles on a volume element mesh. The former approach, where particles are positioned on a cubic lattice structure, is widely used in particle-based methods community. For example, Dominguez et al.[24] proposed a pre-processing tool for their DualSPHysics library, where particles are generated on lattice structure and 3-D object is represented by particle model with excluding the outside particles. This approach has the advantage that particles are equalized, therefore, the induced particles distribution is isotropic. However, portraying the correct surface in particular for complex geometry requires a very fine spatial resolution. The second approach, where particles are generated at the center of tetra- or hexahedron volume elements and its volume is equal to the corresponding element volume, is widely used in the application of bird strike[25-26] and provided by state-of-art commercial pre-processing tools. The approach can accurately portray the complex surface, however, comprises drawbacks of non-uniform

* **Biography:** Yujie Zhu (1992-), Male, Ph. D. Candidate,
E-mail: yujie.zhu@tum.de
Corresponding author: Chi Zhang, Xiangyu Hu,
E-mail: c.zhang@tum.de, xiangyu.hu@tum.de

particle spacing and volume which reduce the interpolation accuracy. Recently, the weighted Voronoi tessellation (WVT) method has been applied for generating initial particle distribution by Diehl et al.[27] for SPH astrophysical simulation and by Siemann and Ritt[17] for SPH modeling of bird-strike. Also, Vela et al.[28] proposed an algorithm for constructing complex initial density distributions with low noise. More recently, Fu and Ji[29] applied centroidal Voronoi particle method by combining the centroidal Voronoi tessellation and Voronoi particle dynamics for generating isotropic particle distribution for two-dimensional simple geometry. These methods are easy to implement and typically generate optimal particle configuration with very good interpolation properties, however, they need ghost particle to impose proper boundary conditions which hinders the ability of handling complex geometry where ghost particle construction is not an easy task. Notwithstanding the aforementioned efforts, generating isotropic particle distribution for arbitrarily complex 3-D geometry is still in its infancy.

In this paper, we propose a computer-aided design (CAD) compatible body-fitted particle generator, named CAD-BPG thereafter, to generate body-fitted and homogeneous particle distribution for 3-D arbitrarily complex geometry. The key idea is to parse a CAD geometry representation and then conduct particle relaxation with surface bounding governed by the transport-velocity formulation in SPH methodology. More precisely, the CAD-BPG represents an arbitrarily complex geometry by parsing a CAD model, and describes the corresponding geometry surface by constructing an implicit zero level-set function. Starting from a preconditioned lattice particle distribution generated inside the domain of the geometry, a physics-driven relaxation process is introduced to relax particle distributions by applying the transport-velocity formulation[30, 13]. Instead of applying ghost particle as in Ref. [29], we introduce a simple surface bounding method to constrain surface particles to achieve body-fitted particle distribution. Compared with Refs. [24, 29, 27], the present CAD-BPG can achieve body-fitted particle distribution for arbitrarily complex 3-D geometry. The particle distributions for structures, e.g., propeller, stents and anatomical heart model, are generated to demonstrate the simplicity, accuracy and versatility of the proposed CAD-BPG for arbitrarily complex 3-D geometry. Then, the CAD-BPG is applied for modeling wave-structure interaction, where regular wave interacting with an oscillating wave surge converter (OWSC) is considered, and the results show that the present method not only provides an efficient and easy-to-implement pre-processing tool for particle-based simulation but also improves the numerical accuracy compared with lattice particle distribution. Having the validation and implementation, it is not hard to conclude that the CAD-BPG sheds light on particle-based simulation for real-world industrial and engineering applications.

The code of the present particle generator and geometries adopted in this work are available in our open-source SPHinXsys library[31] on GitHub at https://github.com/Xiangyu-Hu/SPHinXsys.

1. Geometry definition and level-set method

In this section, we first briefly present the surface presentation and its parsing of arbitrary complex 3-D geometry. Subsequently, this surface presentation is exploited for constructing a signed-distance level-set function which is applied for surface particle bounding in the physical relaxation process.

1.1 *Surface representation*

To represent the surface of an arbitrary complex 3-D geometry, one very flexible method is the triangulation of the surface. The surface can be approximated to an arbitrary accuracy by adjusting the spatial resolution of the triangles applied. As a well explored topic, the generation of such triangulations has widely applied in CAD modeling, computer graphics and recently as representation of 3D printing geometries. There are many different file formats, e.g. STL, OBJ and VTK, to save such a triangulation and herein we choose STL file format for the surface representation.

For reading and parsing the STL file, we apply a parser provided by Simbody, an open-source library for multi-body dynamics[32] and is coupled with our SPHinXsys library for soling fluid-multi-body interaction problems[20]. More importantly, Simbody also provides several built-in functions, for example finding the distance from a given point to the surface and determining whether a given point is located inside a geometry surface, and these functions play key role in constructing level-set function. Note that one can build its own CAD-model parser or apply a proper open-source library.

1.2 *Level-set method*

Following the level-set method[33], the geometry surface can be represented by the zero level-set of the signed-distance function

$$\Gamma = \{(x,y,z) \,|\, \phi(x,y,z,t) = 0\} \tag{1}$$

Then, the normal direction $\boldsymbol{N} = (n_x, n_y, n_z)^{\mathrm{T}}$ of the surface can be computed from

$$\boldsymbol{N} = \frac{\nabla\phi}{|\nabla\phi|} \tag{2}$$

In present work, a Cartesian background mesh is generated in the whole computational domain to discretize the level-set function. For each mesh cell, the level-set value ϕ is equal to the distance from the cell center to the geometry surface. Also, the negative phase with $\phi < 0$ is defined if the cell center is inside the geometry and positive phase with $\phi > 0$ other- wise. Here, computing the distance from a given point i.e., the cell center, to the corresponding surface and checking whether a point is inside the geometry are conducted by calling built-in functions in Simbody library. Notwithstanding, the distance can be com- puted by iterating all triangles to find the nearest triangle and then find the closest point located on the triangle. Also, the checking procedure can be conducted by checking the sign of the dot product between the nearest triangle's norm and the vector pointing from the closest point located on the triangle to the given point.

2. Model equations and numerical algorithm

In this section, we briefly summarize the model equations for physics-driven relaxation and their corresponding SPH discretization. Then, the particle initial condition and evolution strategies are also presented.

2.1 *Governing equations and physics-driven relaxation*

In present work, the physics-driven relaxation is governed by the conservation of momentum

$$\frac{\mathrm{d}\boldsymbol{v}}{\mathrm{d}t} = \boldsymbol{F}_p \tag{3}$$

where $\boldsymbol{v}$ is the advection velocity, $\boldsymbol{F}_p$ denotes the accelerations due to the repulsive pressure force. Also, $\mathrm{d}(\cdot)/\mathrm{d}t = \partial(\cdot)/\partial t + \boldsymbol{v}\cdot\nabla(\cdot)$ stands for material derivative. Different with the work of Fu et al.[34], the continuity equation is not taken into consideration herein as a homogeneous particle distribution can be obtained by applying the transport-velocity formulation[30, 13, 35] with constant density. Therefore, the pressure term in the right-hand-side (RHS) of Eq. (3) can be computed as

$$\boldsymbol{F}_{p,i} = -\frac{2}{m_i}\sum_j V_i V_j p_0 \nabla_i W_{ij} \tag{4}$$

where m is the particle mass, V the particle volume, p_0 the constant background pressure and $\nabla_i W_{ij}$ represents the gradient of the kernel function $W(|\boldsymbol{r}_{ij}|, h)$ with respect to particle i. Here, $\boldsymbol{r}_{ij} = \boldsymbol{r}_i - \boldsymbol{r}_j$ and h is the smoothing length. As the density is constant and equals to unit, we set p_0 equal to unit for simplicity.

With the acceleration induced by the constant background pressure, the particle evolution is defined by

$$\boldsymbol{r}^{n+1} = \boldsymbol{r}^n + \mathrm{d}\boldsymbol{r} = \boldsymbol{r}^n + \frac{1}{2}\boldsymbol{a}^n \Delta t^2 \tag{5}$$

where $\boldsymbol{a}^n = \boldsymbol{F}_p^n$. Note that only the instant acceleration is considered for the particle evolution and the particle velocity is set to zero at the beginning of each time step to achieve a fully stationary state following Refs. [30, 13, 34]. For numerical stability, the time-step size Δt is constrained by the body force criterion

$$\Delta t \le 0.25\sqrt{\frac{h}{|\mathrm{d}\boldsymbol{v}/\mathrm{d}t|}} \tag{6}$$

For uniform particle distributions, the acceleration induced by the background pressure would vanish due to

$$\sum_j V_j \nabla_i W_{ij} = \boldsymbol{0} \tag{7}$$

the satisfactory of 0th-order consistency, as shown in Eq. (4). Otherwise, the non-vanishing contribution of the repulsive pressure force leads an equilibrium particle distribution by relaxation[30, 35, 13, 34]. After adopting a suitable boundary condition, a body-fitted isotropic particle distribution for arbitrary geometry can be thus achieved.

2.2 *Particle initial condition and evolution strategies*

As introduced in the previous section, a Cartesian lattice grid with specific grid spacing is first generated in the whole computational domain. Subsequently, the particle initial condition can be constructed by generating one particle at the cell center if this cell is located inside the geometry as shown in Fig. 1(a). As observed, the initial particles distribution is not in a body-fitted configuration.

With the physics-driven relaxation, all particles are governed by Eq. (3) to achieve homogeneous particle distribution. However, for particles near the surface, boundary treatment is essential to achieve body-fitted feature. In Ref. [34], a dynamic ghost-particle method enforcing symmetry conditions at all domain boundaries is adopted. However, constructing ghost particles for complex geometry is very challenge. In this work, we introduce a simple surface

particle bounding method. For each particle, its level-set value ϕ_i and normal direction $\boldsymbol{N}_i$ can be interpolated from the background mesh using trilinear interpolation method

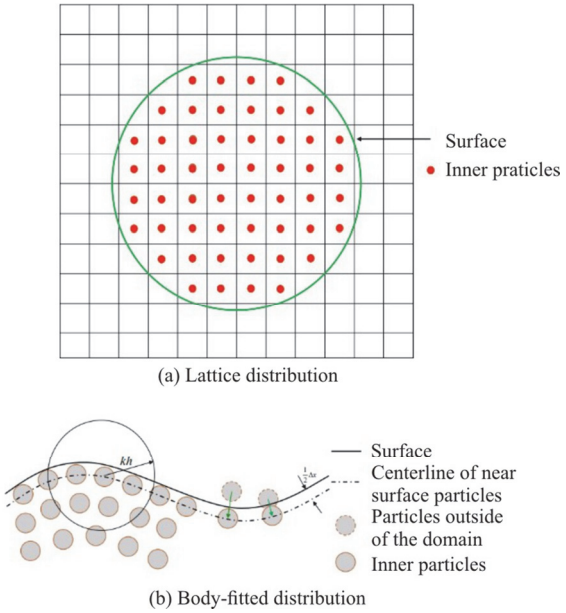

Fig. 1 (Color online) Lattice particle distribution and an illustration of surface particles bounding

$$\phi_i = \phi(\boldsymbol{r}_i), \quad \boldsymbol{N}_i = \boldsymbol{N}(\boldsymbol{r}_i) \tag{8}$$

If the particle satisfies the condition of $\phi_i \geq -1/2\Delta x$, where Δx denotes the initial particle spacing, its position will be updated according to

$$\boldsymbol{r}_i = \boldsymbol{r}_i - \left(\phi_i + \frac{1}{2}\Delta x\right)\boldsymbol{N}_i, \quad \phi_i \geq -\frac{1}{2}\Delta x \tag{9a}$$

$$\boldsymbol{r}_i = \boldsymbol{r}_i \quad \text{otherwise} \tag{9b}$$

as shown in Fig. 1(b). By applying the bounding method, particles near the surface are enforced to locate on geometry surface and a body-fitted particle distribution is achieved accordingly. Note that, the surface particles are relocated at $\phi = -1/2\Delta x$ instead of $\phi = 0$ implying the material interface in the simulation assumed to be located at $\phi = 0$.

2.3 *Implementation*

In summary, the proposed CAD-BPG consists of the following steps.

(1) Geometry representation in CAD model, in STL format herein, is read and parsed for geometry presentation.

(2) The geometry surface is described implicitly with the level-set function based on a Cartesian background mesh. The level-set field is given by the shortest distance from cell center to the geometry surface, and the corresponding sign is determined by checking whether the cell is inside the geometry.

(3) A preconditioned lattice particle distribution is generated. Then, a physics-driven relaxation process is conducted by imposing the proposed surface bounding method.

The detailed flowchart of the proposed CAD-BPG is outlined in Algorithm 1 (Table 1). It is easy to see that the physics-driven process of the proposed method is almost the same with the SPH for fluid dynamics. This particle generator is simple and can be implemented into an existing SPH code straightforwardly. Also note that the kernel function adopted in this algorithm should be the same with that of the SPH method in real simulation and thus the 0th-order consistency as shown in Eq. (7) of the particle approximation can be achieved. According to our test, the body-fitted particle distribution can be generated within 100 steps relaxation as shown in Section 3.1.

Table 1 Algorithms of the proposed CAD-BPG

Algorithm 1
1. Setup parameters and initialize the physics-driven relaxation
2. Read and parse the polygon mesh of a specific geometry from CAD files
3. Initialize the background Cartesian mesh and the level-set function
4. Generate a preconditioned lattice particle distribution
5. **While** simulation termination condition is not satisfied do
6. Calculate the pressure force $\boldsymbol{F}_p$ (Eq. (4))
7. Set the time-step Δt (Eq. (6))
8. Update particles position $\boldsymbol{r}^{n+1}$ (Eq. (5))
9. Interpolate the attribute function ϕ_i and the corresponding normal direction $\boldsymbol{N}_i$ of each particle (Eq. (8))
10. Constrain outside particles onto surface (Eq. (9))
11. Update the particle-neighbor list and kernel values and gradient
12. Update the particle configuration
13. **End**
14. Terminate the physics-driven relaxation

3. Examples

In this part, we first test the proposed CAD-BPG for a simple sphere and validate its accuracy by the convergence analysis of L2-norm error. Subsequently, the CAD-BPG is applied for generating particle distribution for complex structure including propeller, stents and anatomical heart model. Finally, the CAD-BPG is implemented as a pre-processing tool for modeling regular wave interaction with an OWSC and the predicted surface elevation, flap rotation and pressure loads are compared with experimental data. The 5th-order C2 Wendland[36] is applied and the

smoothing length is set as $h = 1.05\Delta x$ with Δx denoting the initial particle spacing for all cases. Note that we perform the physics-driven relaxation starting from a random particle distribution rather than the lattice one to demonstrate the robustness of the present method. Also, the background mesh for level-set field is only established within a narrow band of the geometry interface to save storage memory.

3.1 *Sphere*

A sphere with radius $R = 40$ as shown in Fig. 2(a) is first considered. Imported from an external STL file, the geometry is read and parsed. The established level-set field and the corresponding geometry surface are given in Fig. 2(b). Although this geometry is simple, it is still difficult to generate a body-fitted uniform particle distribution for traditional methods. In this test, three resolutions with $\Delta x = R/20$, $\Delta x = R/40$ and $\Delta x = R/80$ are adopted.

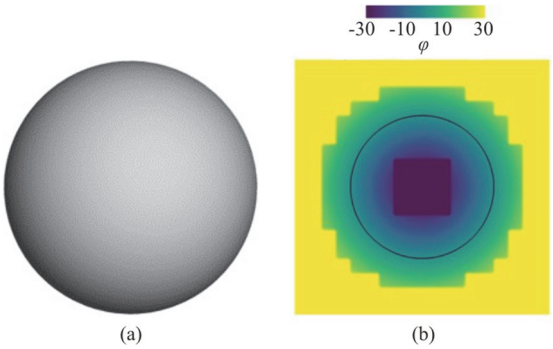

Fig. 2 (Color online) Sphere: (a) Visualization of CAD geometry in STL format and (b) sliced view of the level-set field

Figure 3 shows the lattice and relaxed particle generations of the sphere at the resolution of $\Delta x = R/20$. We can observe that the lattice particle distribution cannot represent the exact geometry. However, as shown in Fig. 3(c) and the corresponding slice view, the proposed CAD-BPG gives a most realistic representation of the geometry even though the particle evolution starts from a random distribution. Figure 4 gives the particle distribution for two higher resolutions. It is obvious that the particle generated by CAD-BPG is body-fitted and uniformly distributed. The averaged L2-norm distance D_{avg} between surface particles and the surface and the averaged particle kinetic energy are presented in Figs 5(a) and 5(b), respectively. At the beginning, particles distribution is not body-fitted and the distance between surface particle and the surface is large especially for the one with lower resolution. After several steps of relaxation, the distance is approaching to zero and the kinetic energy is tending to stable. Note that the averaged particle kinetic energy is not vanished in stable state which is caused by the non-vanishing repulsive force for surface particles. Besides, we want to emphasize that the present CAD-BPG can achieve the almost equilibrium state less than 100 steps in this case demonstrating its efficiency.

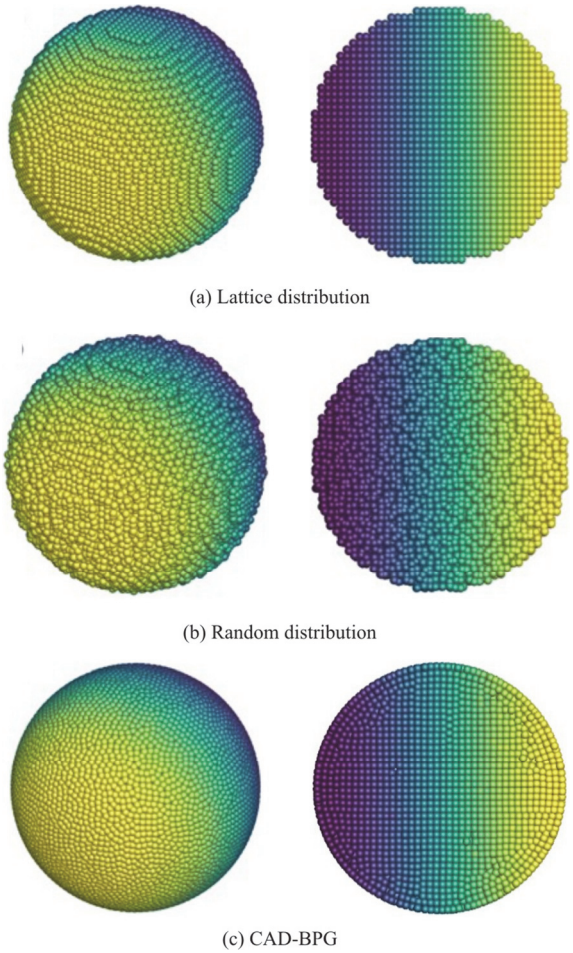

Fig. 3 (Color online) Particle distributions with spatial resolution of $\Delta x = R/20$ and their sliced view (right panel) for sphere

3.2 *Applications in complex structure*

In this part, the CAD-BPG is implemented for generating particle for complex structure which are ubiquitous in industrial and biomechanical applications. Firstly, we consider a propeller structure which consists of 12 sharp blades as shown in Fig. 6(a). This structure is very challenging due to its complex geometry and blade's sharp nature. Figure 6 shows the body-fitted particle distribution for the propeller with 955 450 total particles in different points of view. It can be noted that the present CAD-BPG can generate a well-regularized particle distribution for this complex geometry and reproduce the sharp blades well. To the best knowledge of the authors, this is the first

body-fitted particle distribution generated for propeller structure. In the future work, this propeller model will be used for studying the fluid interaction with propeller structure which is our ongoing work.

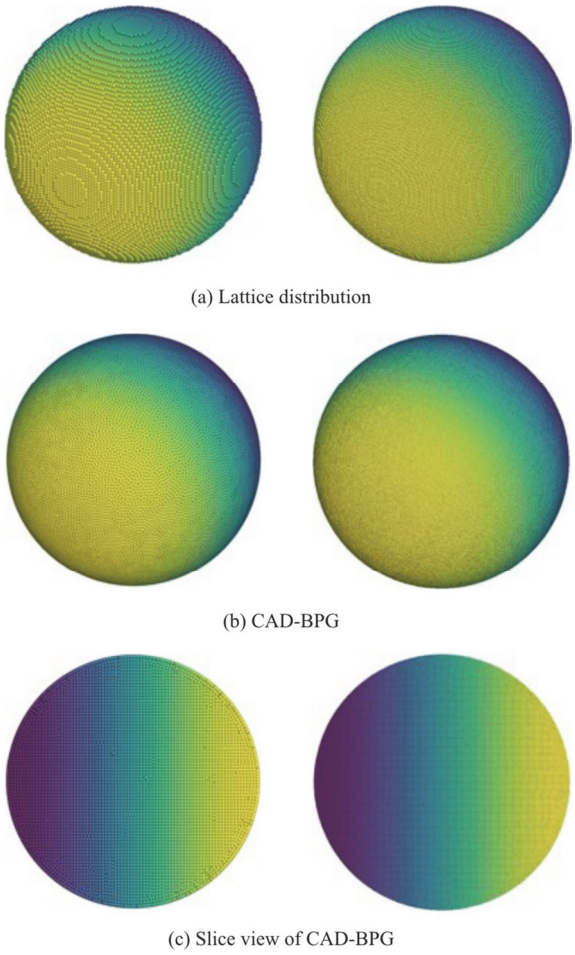

Fig. 4 (Color online) Particle distributions with two higher spatial resolutions ($\Delta x = R / 40$ (left panel), $\Delta x = R / 80$ (right panel)) for sphere

Secondly, we consider two realistic cardiovascular stent structures, i.e., Palmaz-Schatz shaped (PS-shaped) stent and Cypher shaped (C-shaped) stent, which are widely used in clinical applications. In recent years, considerable amount of FEM-based researches have been carried out in order to improve the quality and feasibility of stents. However, particle-based research has not been conducted due to the lack of body-fitted particle distribution on them.

Figure 7 shows the CAD geometry of PS-shaped stent and the corresponding body-fitted particle distribution with total 226 775 particles generated by the present CAD-BPG. It is clear that the geometry is well represented and particles are uniformly distributed. For the C-shaped stent, the CAD geometry as well as the corresponding particle distribution with total 45 644 particles are presented in Fig. 8. Again, a body-fitted particle distribution is achieved.

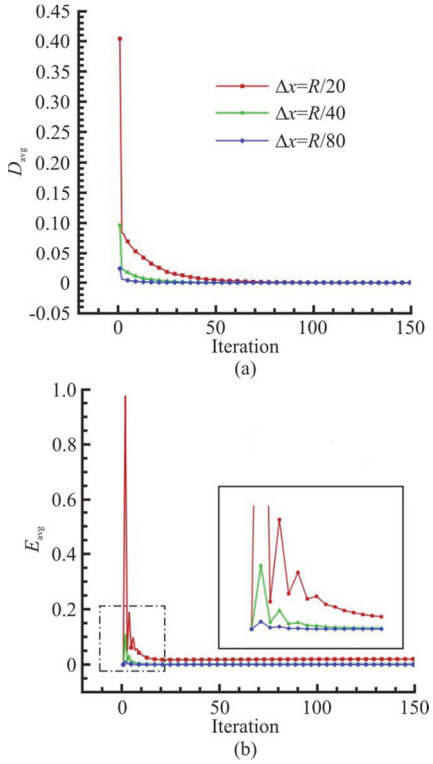

Fig. 5 (Color online) Sphere: (a) Averaged L2-norm distance between surface particles and physics surface and (b) averaged particle kinetic energy

Numerical modeling of the human heart and its function can help us understand various cardiac diseases as noted in Ref. [37]. In our recent work of Ref. [22] an integrative SPH method for addressing the simulation of the principle aspects of cardiac function, including cardiac electrophysiology, passive mechanical response and electromechanical coupling, is presented. For total heart modeling where complex geometry is involved, body-fitted particle distribution is essential for numerical accuracy. In the last but not least case, we consider a total heart model which consists of four chambers. Its CAD geometry and the body-fitted particle distribution with 500091 total particles are shown in Fig. 9. It can be noted that a well-regularized particle distribution is produced demonstrating that the present CAD-BPG can handle very complex geometries. Note that the stent and heart model will be used in our future work concerning the modeling of total heart function.

3.3 *Wave interaction with an oscillating wave surge converter*

In this section, we implement the proposed CAD- BPG as a pre-processing tool for the modeling of wave interaction with an OWSC. Following the experimental work of Wei et al.[38], the schematic of

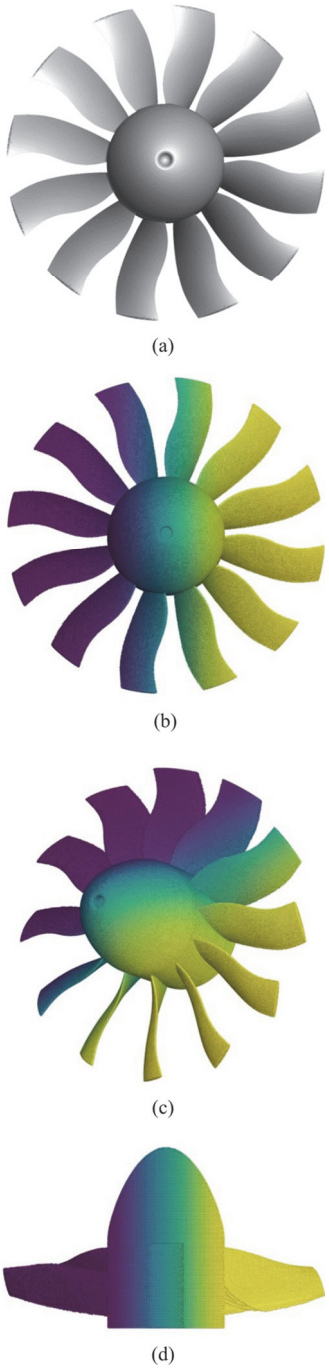

Fig. 6 (Color online) Propeller: (a) Visualization of CAD geometry in STL format, (b) particle distribution by CAD-BPG, (c) one side view of CAD-BPG, (d) another side view of CAD-BPG

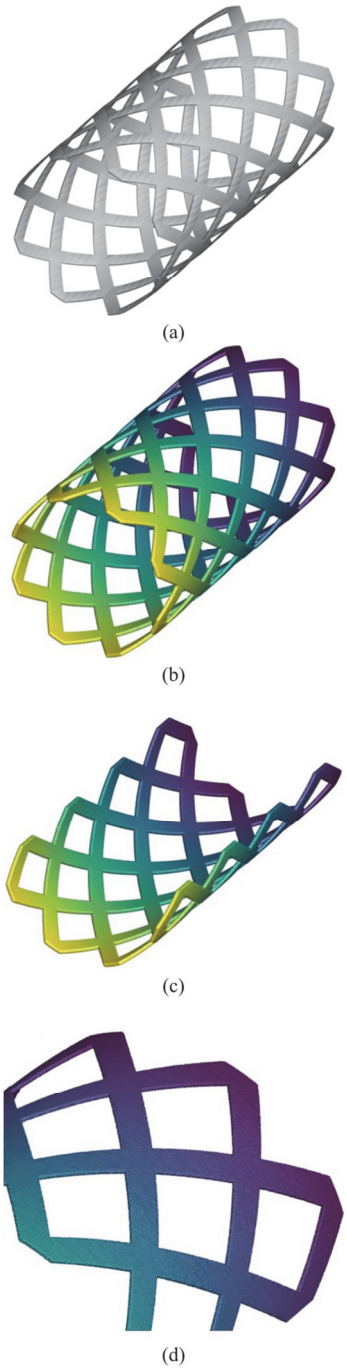

Fig. 7 (Color online) Palmaz-Schatz shaped stent: (a) Visualization of CAD geometry in STL format, (b) particle distribution by CAD-BPG, (c) sliced view of CAD-BPG, (d) a zoom of CAD-BPG

the numerical setup is shown in Fig. 10. Here, the OWSC device is simplified as a 1.04 m×0.48 m×0.12 m box-type flap hinged to a 0.16 m high base. The mass of the flap is 33 kg and the inertia of the flap is 1.84 kg·m^2. One wave probe termed as WP04 located at $x = 3.99$ m and four pressure sensors whose positions are given in Table 2 are used to measure the time histories of the surface elevation and pressure loads on the flap. Note that the pressure sensors and wave probe are termed identical to those of the experiment in Ref. [38] for clarity.

In this case, both the body-fitted particle distribution and the lattice one are considered. Figure 11 presents the boundary-representation of the tank, wave

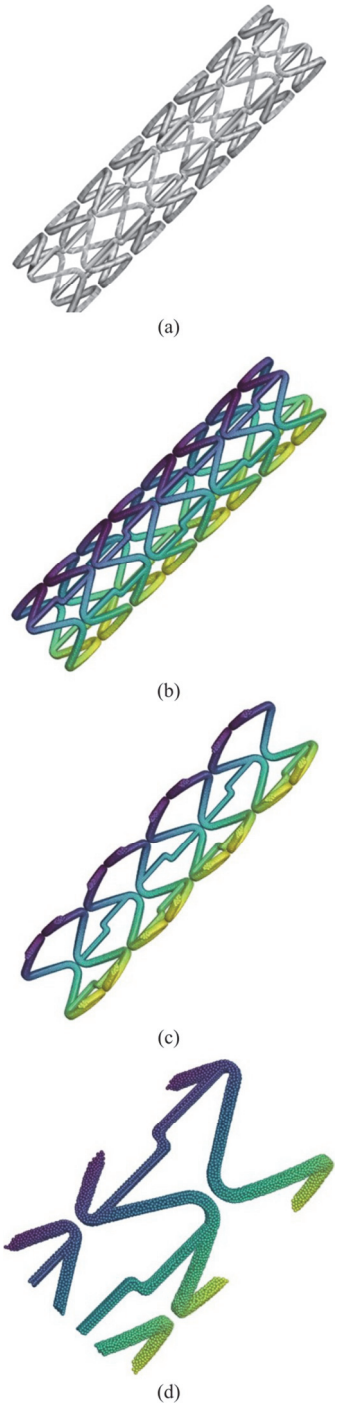

Fig. 8 (Color online) Cypher shaped stent: (a) Visualization of CAD geometry in STL format, (b) particle distribution by CAD-BPG, (c) sliced view of CAD-BPG, (d) a zoom of CAD-BPG

maker and flap as well as their corresponding particle distributions generated by the present CAD-BPG. For both tests, the initial particle space is set as $\Delta x = 0.03$ m resulting in a number of 1.542×10^6 fluid particles and 0.628×10^6 solid particles (including tank, wave maker and flap).

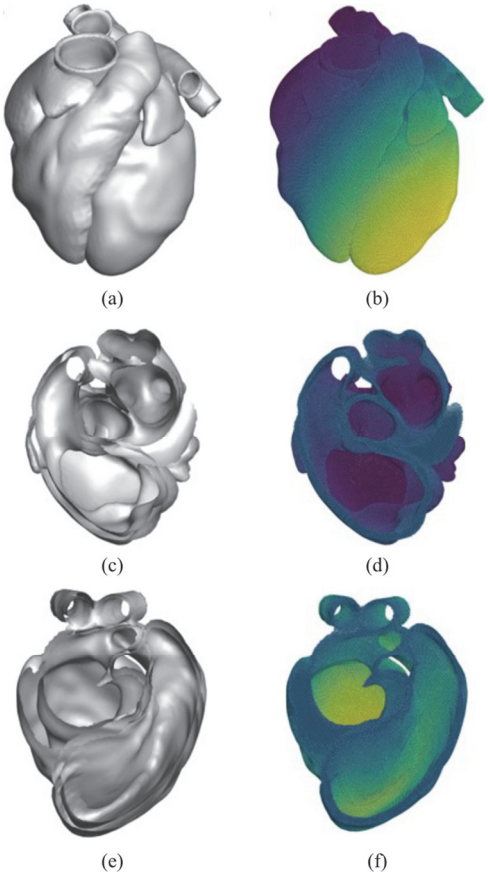

Fig. 9 (Color online) Lv-heart: (a) Visualization of CAD geometry in STL format, (b) particle distribution by CAD-BPG, (c) one sliced view of CAD geometry, (d) sliced view of CAD-BPG corresponding to (c), (e) another sliced view of CAD geometry, (f) sliced view of CAD-BPG corresponding to (e)

The regular wave can be generated by imposing a piston–type wave maker whose displacement is determined by the linear wave making theory

$$\boldsymbol{r} = S\sin(ft + \phi) \tag{10}$$

where S is the wave stroke, f the wave frequency and ϕ the initial phase. Here, the wave stroke S is determined by

$$S = \frac{H\sinh(2kh_0) + 2kh_0}{\sinh(2kh_0)\tanh(kh_0)} \tag{11}$$

where H is the wave height, h_0 the water depth and k is the wave number. We consider the regular wave interaction with OWSC in condition of wave height $H = 5$ m and wave period $T = 10$ s in full scale.

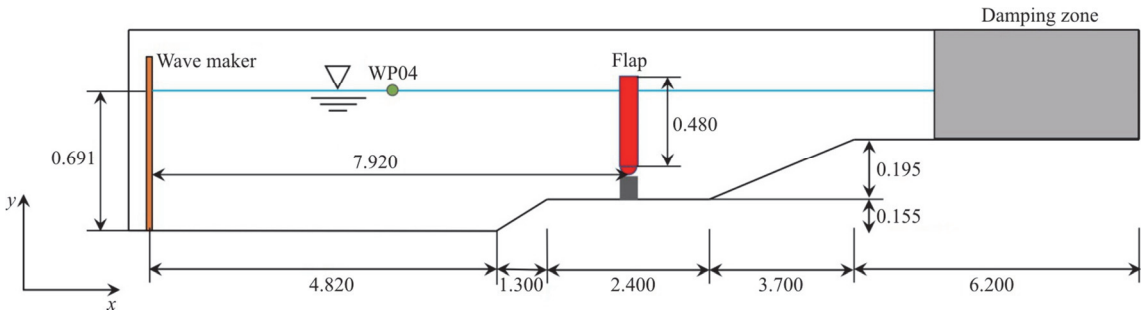

Fig. 10 (Color online) Schematic of the wave tank and the OWSC model. The scale is 1 : 25 (m)

Table 2 Positions of the pressure sensors on the front flap face. The position along the z-axis is measured from the center of the device, and $y = 0$ denotes the mean water level

No.	y-axis/m	z-axis/m
PS01	–0.046	–0.468
PS03	0.050	0.364
PS05	–0.300	0.364
PS13	0.025	0.052

For the wave interaction with the flap, the total force and torque acting about the center of mass of the solid body can be expressed as

$$\boldsymbol{F} = \sum_{a \in N} \boldsymbol{f}_a, \quad \boldsymbol{\tau} = \sum_{a \in N} (\boldsymbol{r}_a - \boldsymbol{r}_{com}) \times \boldsymbol{f}_a \tag{12}$$

where $\boldsymbol{r}_{com}$ is the center of mass, $\boldsymbol{f}_a$ denotes the fluid force action on a flap particle a located at $\boldsymbol{r}_a$. The total force and torque are obtained to solve the Newton-Euler equation

$$\begin{pmatrix} \boldsymbol{F} \\ \boldsymbol{\tau} \end{pmatrix} = \begin{pmatrix} m\mathbb{I} & 0 \\ 0 & \boldsymbol{I} \end{pmatrix} \begin{pmatrix} \dfrac{\mathrm{d}\boldsymbol{v}}{\mathrm{d}t} \\ \dfrac{\mathrm{d}\boldsymbol{\Omega}}{\mathrm{d}t} \end{pmatrix} \tag{13}$$

where m is the mass of flap, $\mathbb{I}$ the identity matrix, $\boldsymbol{I}$ the moment of inertia about the center of mass and $\boldsymbol{\Omega}$ is the angular velocity. Here, only the rotation is taken into consideration for the motion of the flap.

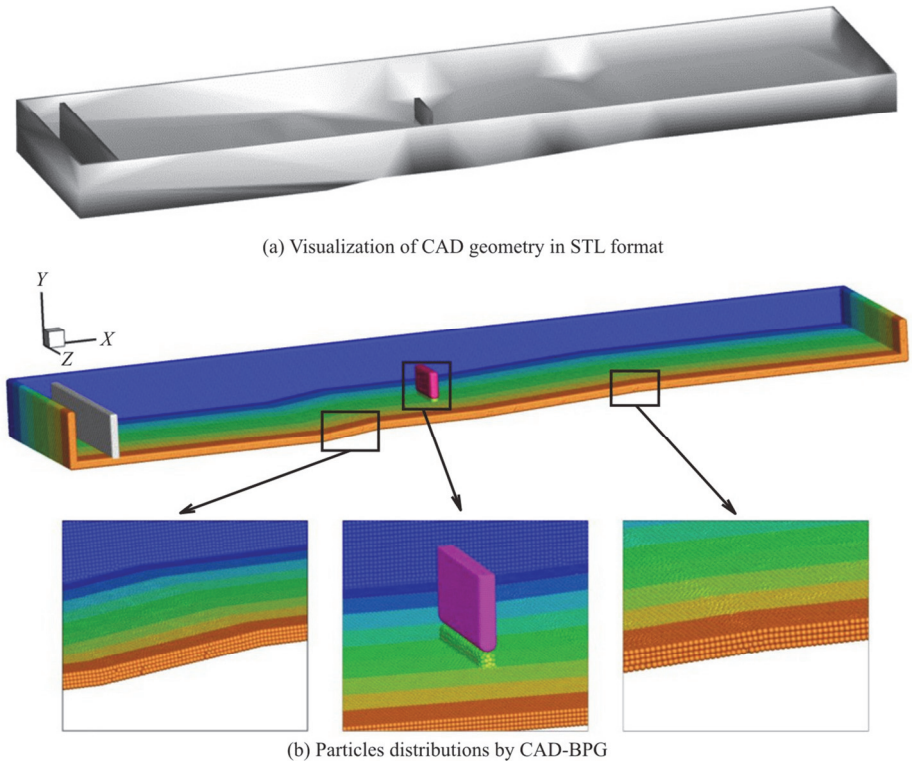

(a) Visualization of CAD geometry in STL format

(b) Particles distributions by CAD-BPG

Fig. 11 (Color online) Modeling of wave interaction with OWSC: (a) Visualization of CAD geometry in STL format and (b) particles distributions by CAD-BPG

Figure 12 presents several snapshots showing the free surface colored by velocity magnitude and the flap's rotation predicted by using the body-fitted particle distribution as initial condition. It can be observed that smooth velocity fields are produced even complex interactions between wave and the flap are involved. Also, wave refection and breaking can be noted in the region near the flap during the interaction.

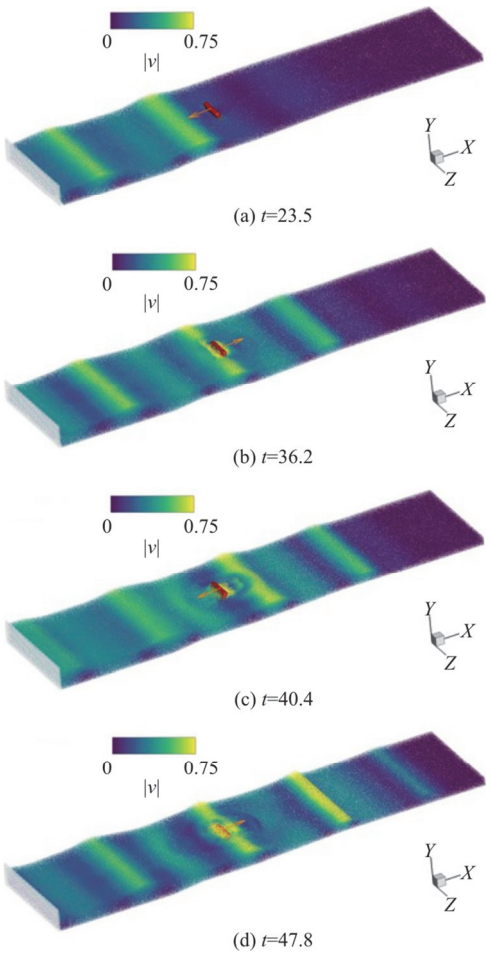

Fig. 12 (Color online) Modeling of wave interaction with OWSC: Free surfaces with particles colored by velocity magnitude and the flap motion predicted by body-fitted particle distribution for wave height $H = 5$ m and wave period $T = 10$ s

Figure 13 shows the comparison of the time history of surface elevation at probe WP04 and the corresponding flap rotation between experimental data and numerical results obtained by the lattice and body-fitted particle distributions. For wave elevation as shown in Fig. 13(a), both results have good agreement with experimental data while the body-fitted particle initial condition shows improved accuracy in modeling of wave dynamics. This may due to the fact that body-fitted particle distribution of the tank's slope parts significantly improve the accuracy of fluid-solid interaction. Again, the body-fitted particle distribution shows impressive improvement in predicting the large amplitude rotation of the flap as shown in Fig. 13(b).

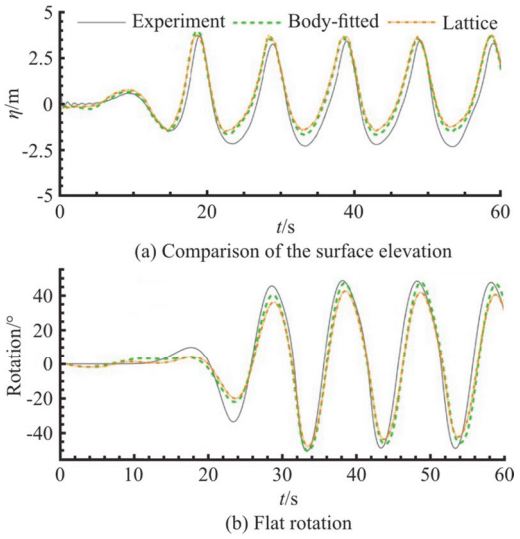

Fig. 13 (Color online) Modeling of wave interaction with OWSC: Comparison of the surface elevation (top panel) and flap rotation (bottom panel) for wave height $H = 5$ m and wave period $T = 10$ s

Figure 14 shows the time histories of the pressure signals recorded by the pressure sensors given in Table 2. Note that the initial hydrostatic pressure is subtracted from the recorded pressure signals inducing negative drops in some profiles as Ref. [38]. Compared with the experimental data, the main plateaus of all the pressure profiles are reasonably well captured by both particle distributions. For sensors PS01 and PS03, large pressure peaks and drops are noted since the present SPH model is based on weakly-compressible assumption and air cushion effects are not captured in mono-fluid simulation. Similar to the results reported in Ref. [38], the pressure drops for sensors PS05 and PS13 are underestimated in present results and theses discrepancies are related to the wave breaking. Also, the pressure signals show identical profile for both particle distributions indicating that the initial particle distribution has small effects on the pressure field.

4. Conclusion

In this paper, we present a CAD-compatible body-fitted particle generator for arbitrarily complex 3-D geometry and apply it as a pre-processing tool for modeling of wave-structure interaction. This particle generator mainly includes the following procedures: (1) the geometry information is accessed by importing

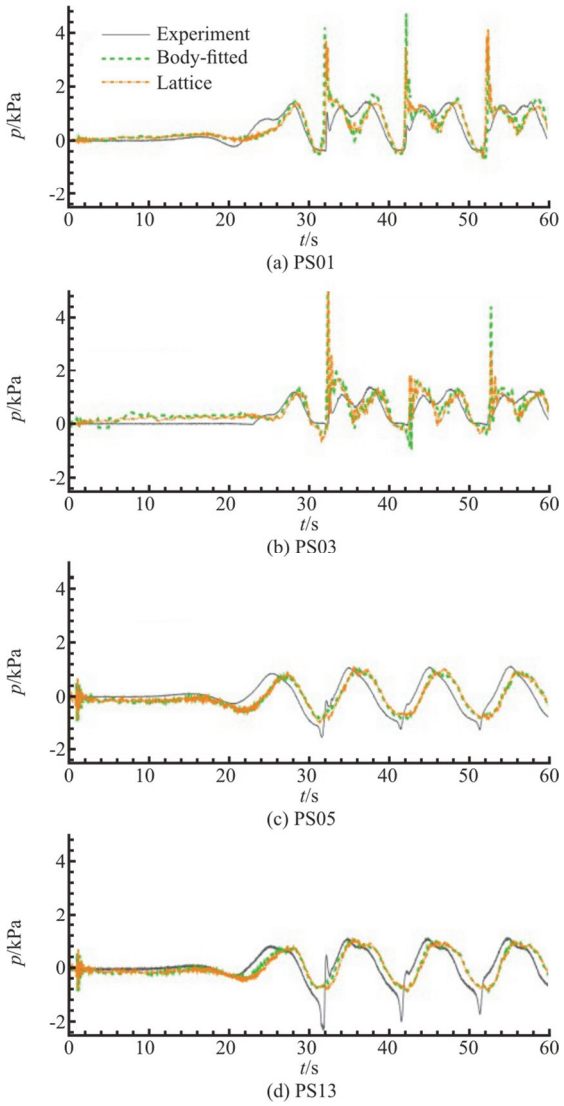

Fig. 14 (Color online) Modeling of wave interaction with OWSC: Comparison of the time histories of wave loads on the flap for wave height $H = 5$ m and wave period $T = 10$ s

and parsing the polygon mesh storing in external CAD files, and the geometry surface is then described by an implicit zero level-set function, (2) starting from a preconditioned lattice or random particle distribution, particles evolution is driven by a constant background pressure under the framework of WCSPH methodology, (3) surface particles are constrained by introducing an efficient surface bounding method to achieve body-fitted feature. With the assumption that each particle possesses an invariant volume, a body-fitted well-regularized particle distribution can be achieved when system approaches to stable state. A number of benchmark cases with complex geometry demonstrate that the particle distribution generated by the present CAD-BPG represents the geometry well and particles are uniformly distributed. Then, the improvements of computational accuracy by adopting the present CAD-BPG are proved by a physical implementation. In addition, the present approach is CAD-compatible and can read arbitrarily complex geometry from external CAD files implying a promising potential of particle-based methods in real-world applications.

Acknowledgements

The work was supported by the National Natural Science Foundation of China (Grant No. 91952110), the Deutsche Forschungsgemeinschaft under (Grant Nos. DFG HU1572/10-1, DFG HU1527/12-1).

References

[1] Gingold R. A., Monaghan J. J. Smoothed particle hydrodynamics: Theory and application to non-spherical stars [J]. *Monthly Notices of the Royal Astronomical Society*, 1977, 181(3): 375-389.

[2] Lucy L. B. A numerical approach to the testing of the fission hypothesis [J]. *The Astronomical Journal*, 1977, 82: 1013-1024.

[3] Koshizuka S., Oka Y. Moving-particle semi-implicit method for fragmentation of incompressible fluid [J]. *Nuclear Science and Engineering*, 1996, 123(3): 421-434.

[4] Mishra B. K., Rajamani R. K. The discrete element method for the simulation of ball mills [J]. *Applied Mathematical Modelling*, 1992, 16(11): 598-604.

[5] Monaghan J. J. Simulating free surface flows with SPH [J]. *Journal of Computational Physics*, 1994, 110(2): 399-406.

[6] Hu X. Y., Adams N. A. A multi-phase SPH method for macroscopic and mesoscopic flows [J]. *Journal of Computational Physics*, 2006, 213(2): 844-861.

[7] Monaghan J. J. SPH without a tensile instability [J]. *Journal of Computational Physics*, 2000, 159(2): 290-311.

[8] Zhang C., Hu X. Y., Adams N. A. A weakly compressible SPH method based on a low-dissipation Riemann solver [J]. *Journal of Computational Physics*, 2017, 335: 605-620.

[9] Zhang C., Xiang G. M., Wang B. et al. A weakly compressible SPH method with WENO reconstruction [J]. *Journal of Computational Physics,* 2019, 392: 1-18.

[10] Benz W., Asphaug E. Simulations of brittle solids using smooth particle hydrodynamics [J]. *Computer Physics Communications*, 1995, 87(1-2): 253-265.

[11] Libersky L. D., Petschek A. G. Smooth particle hydrodynamics with strength of materials (Larry D., Libersky A., Petschek G. Advances in the free-Lagrange method including contributions on adaptive gridding and the smooth particle hydrodynamics method) [M]. Berlin, Heidelberg, Germany: Springer, 1991, 248-257.

[12] Randles P. W., Libersky L. D. Smoothed particle hydrodynamics: Some recent improvements and applications [J]. *Computer Methods in Applied Mechanics and Engineering*, 1996, 139(1-4): 375-408.

[13] Zhang C., Hu X., Adams N. A. A generalized transport-velocity formulation for smoothed particle hydrodynamics [J]. *Journal of Computational Physics*, 2017, 337: 216-232.

[14] Ye T., Pan D., Huang C. et al. Smoothed particle hydro-

dynamics (SPH) for complex fluid flows: Recent developments in methodology and applications [J]. *Physics of Fluids*, 2019, 31(1): 011301.

[15] Zhang C., Rezavand M., Hu X. A multi-resolution SPH method for fluid-structure interactions [J]. *Journal of Computational Physics*, 2021, 429: 110028.

[16] Gotoh H., Khayyer A. On the state-of-the-art of particle methods for coastal and ocean engineering [J]. *Coastal Engineering Journal*, 2018, 60(1): 79-103.

[17] Siemann M. H., Ritt S. A. Novel particle distributions for SPH bird-strike simulations [J]. *Computer Methods in Applied Mechanics and Engineering*, 2019, 343: 746-766.

[18] Alimirzazadeh S., Kumashiro T., Leguizamón S. et al. GPU-accelerated numerical analysis of jet interference in a six-jet Pelton turbine using finite volume particle method [J]. *Renewable Energy*, 2020, 148: 234-246.

[19] Ji Z., Stanic M., Hartono E. A. et al. Numerical simulations of oil flow inside a gearbox by smoothed particle hydrodynamics (SPH) method [J]. *Tribology International*, 2018, 127: 47-58.

[20] Zhang C., Wei Y., Dias F. et al. An efficient fully Lagrangian solver for modeling wave interaction with oscillating wave energy converter [EB/OL]. arXiv preprint, 2020, arXiv:2012.05323.

[21] Crespo A. J. C., Hall M., Domínguez J. M. et al. Floating moored oscillating water column with meshless SPH method [C]. *ASME 2018 37th International Conference on Ocean, Offshore and Arctic Engineering*, Madird, Spain, 2018.

[22] Zhang C., Wang J., Rezavand M. et al. An integrative smoothed particle hydrodynamics framework for modeling cardiac function [J]. *Computer Methods in Applied Mechanics and Engineering*, 2021, 381: 113847.

[23] Zhang C., Zhu Y., Yu Y. et al. A simple artificial damping method for total Lagrangian smoothed particle hydrodynamics [EB/OL]. arXiv preprint, 2021, arXiv:2102.04898.

[24] Domínguez J. M., Crespo A. J. C., Barreiro A. et al. Development of a new pre-processing tool for SPH models with complex geometries [C]. *6th International SPHERIC workshop*, Hamburg, Germany, 2011, 117-124.

[25] Vignjevic R., Orłowski M., De Vuyst T. et al. A parametric study of bird strike on engine blades [J]. *International Journal of Impact Engineering*, 2013, 60: 44-57.

[26] Heimbs S. Computational methods for bird strike simulations: A review [J]. *Computers and Structures*, 2011, 89(23-24): 2093-2112.

[27] Diehl S., Rockefeller G., Fryer C. L. et al. Generating optimal initial conditions for smoothed particle hydrodynamics simulations [J]. *Publications of the Astronomical Society of Australia*, 2015, 32: e048.

[28] Vela L. V., Sanchez R., Geiger J. ALARIC: An algorithm for constructing arbitrarily complex initial density distributions with low particle noise for SPH/SPMHD applications [J]. *Computer Physics Communications*, 2018, 224: 186-197.

[29] Fu L., Ji Z. An optimal particle setup method with Centroidal Voronoi Particle dynamics [J]. *Computer Physics Communications*, 2019, 234: 72-92.

[30] Adami S., Hu X. Y., Adams N. A. A transport-velocity formulation for smoothed particle hydrodynamics [J]. *Journal of Computational Physics*, 2013, 241: 292-307.

[31] Zhang C., Rezavand M., Zhu Y. et al. SPHinXsys: An open-source meshless, multi-resolution and multi-physics library [J]. *Software Impacts*, 2020, 6: 100033.

[32] Sherman M. A., Seth A., Delp S. L. Simbody: Multibody dynamics for biomedical research [J]. *Procedia IUTAM*, 2011, 2: 241-261.

[33] Osher S., Sethian J. A. Fronts propagating with curvature-dependent speed: Algorithms based on Hamilton-Jacobi formulations [J]. *Journal of Computational Physics*, 1988, 79(1): 12-49.

[34] Fu L., Han L., Hu X. et al. An isotropic unstructured mesh generation method based on a fluid relaxation analogy [J]. *Computer Methods in Applied Mechanics and Engineering*, 2019, 350: 396-431.

[35] Litvinov S., Hu X. Y., Adams N. A. Towards consistence and convergence of conservative SPH approximations [J]. *Journal of Computational Physics*, 2015, 301: 394-401.

[36] Wendland H. Piecewise polynomial, positive definite and compactly supported radial functions of minimal degree [J]. *Advances in computational Mathematics*, 1995, 4(1): 389-396.

[37] Quarteroni A., Lassila T., Rossi S. et al. Integrated heart–Coupling multiscale and multiphysics models for the simulation of the cardiac function [J]. *Computer Methods in Applied Mechanics and Engineering*, 2017, 314: 345-407.

[38] Wei Y., Rafiee A., Henry A. et al. Wave interaction with an oscillating wave surge converter, part I: Viscous effects [J]. *Ocean Engineering*, 2015, 104: 185-203.